Soft Matter

PAPER

View Article Online
View Journal | View Issue

Cite this: *Soft Matter*, 2026, **22**, 1583

Molecular picture of curing and incomplete cross-linking of epoxy at a solid interface

Satoru Yamamoto, *[a] Riichi Kuwahara [b] and Keiji Tanaka *[ac]

Received 30th October 2025,
Accepted 27th January 2026

DOI: 10.1039/d5sm01089f

rsc.li/soft-matter-journal

Understanding the buried interface between silica and epoxy resin is crucial for improving the performance and reliability of epoxy composites and adhesives. Here, molecular dynamics simulations were used to reveal a heterogeneous molecular picture of aggregation and curing at the amorphous silica/epoxy interface. A density increase was observed within 2 nm of the interface, driven by the orientation and packing of epoxy and amine molecules. Smaller amines segregated near the substrate, accelerating interfacial curing in the early stages. However, subsequent reactions slowed due to restricted mobility, resulting in a ~10% lower conversion than in the bulk. Unreacted monomers and isolated fragments accumulated near the interface, indicating adverse effects on adhesion. These findings provide molecular-level insights into buried interfaces and inform strategies for improving adhesion and reliability in epoxy-based composites and adhesives.

1. Introduction

Epoxy resins are produced through the curing reaction between an epoxy base and an amine hardener,[1–7] during which a three-dimensional network structure forms, potentially affecting their mechanical properties and other characteristics.[8–11] They are commonly used as adhesives or as composites with fillers such as silica particles.[12–16] Although cured epoxy products are high-strength and durable materials,[17,18] understanding their adhesion properties to adherends and fillers is crucial for further improving their functionality and reliability.[19–23] Because adhesion is governed by molecular-level organization and interactions at the interface, it is essential to elucidate how the aggregation states of epoxy resins at solid surfaces differ from those in the bulk.[7,24–27] In the bulk, the aggregation states are generally isotropic and homogeneous, whereas at the interface, they are anisotropic and certain components may be segregated. The reason for this lies in both entropic and energetic interactions at the interface between the epoxy resin and the solid.[28,29] Entropically, substances with smaller molecular sizes preferentially accumulate at the interface, while energetically, electrostatic and van der Waals interactions with the adherend surface play an important role.[26]

Spectroscopic techniques such as X-ray photoelectron spectroscopy (XPS),[30] sum-frequency generation (SFG) spectroscopy,[31,32] and neutron reflectivity (NR) measurements[33] are effective experimental approaches to reveal heterogeneous aggregation states at buried interfaces. Segregation of amine compounds at the interface between the epoxy/amine stoichiometric mixture and copper surface was revealed using XPS.[30] Heterogeneity in the curing process of an epoxy resin at the quartz interface was revealed using SFG spectroscopy while the presence of aggregated water between the cured epoxy product and the silicon substrate was elucidated by NR measurements.[33] However, the information obtained is statistical and it is difficult to precisely determine the molecular picture, such as the local orientation of a particular functional group. Because of this difficulty in observing buried interfaces, heterogeneous aggregation states at interfaces are not yet fully understood.

In contrast, with the proper problem setup, molecular dynamics (MD) simulations have the potential to reveal a detailed molecular picture at the interface as well as in the bulk.[34–44] We have successfully calculated the aggregation state and curing reaction at the interface of epoxy resins by MD simulation and revealed the heterogeneity of epoxy resins, which is different from the bulk.[26] The substrates chosen were mostly crystalline structures such as copper, silicon, and quartz.[45–47] However, the surface of aluminum, for example, is covered with an amorphous oxide layer,[48] and silica particles are inherently amorphous,[49] so it is necessary to consider such amorphous solid surfaces if a more realistic system is required. Recently, we proposed a method to create amorphous alumina and silica substrates on which we calculated the aggregation

[a] *Centre for Polymer Interface and Molecular Adhesion Science, Kyushu University, Fukuoka 819-0395, Japan. E-mail: s-yamamoto@cstf.kyushu-u.ac.jp*
[b] *Dassault Systèmes K. K., Tokyo 141-6020, Japan. E-mail: Riichi.KUWAHARA@3ds.com*
[c] *Department of Applied Chemistry, Kyushu University, Fukuoka 819-0395, Japan. E-mail: k-tanaka@cstf.kyushu-u.ac.jp*

state and curing reaction of epoxy resins.[50,51] Although the results obtained were basically the same as those for crystal surfaces, there were some useful findings, such as differences in the roughness of the substrate surfaces. However, those studies did not address the relationship between detailed molecular orientation and reaction kinetics, or the spatially resolved curing behavior. Incorporating these elements allows a more comprehensive molecular picture of interfacial curing to be established.

In this study, MD simulations were conducted to investigate epoxy resins at interfaces with silica particles, which are commonly used as fillers. The aggregation states of an epoxy resin at the amorphous silica interface and the subsequent network formation process were analysed to elucidate the heterogeneous molecular picture near the solid interface. Particular attention was given to the molecular orientation at the outermost interface on the substrate side and its influence on reaction kinetics, as well as to the presence of incompletely cross-linked regions.

2. Simulation method

Diglycidyl ether of bisphenol A (DGEBA) and 4,4′-diaminodiphenylmethane (DDM) were used as epoxy and amine compounds, respectively. Fig. 1(a) shows the chemical structures of epoxy and amine compounds, whereas Fig. 1(b) illustrates the simulation system. A stoichiometric mixture consisting of 360 DGEBA and 180 DDM molecules was placed on an amorphous silica substrate with lateral dimensions of 5 nm, and a vacuum layer was placed on top of the system. The structure of amorphous silica in bulk was obtained by randomly recombining chemical bonds in silicon crystals to create amorphous silicon and inserting oxygen atoms between Si–Si to create Si–O–Si.[50] The density was set to 2.20 g cm^{-3} with reference to experimental values. From the bulk amorphous silica structure, a layer structure with a thickness of 2 nm was cut out, and hydrogen atoms were added to the dangling bonds to create an amorphous silica surface. As a result of the surface construction procedure, both SiOH and SiH groups were present on the surface. Although silica surfaces are generally described as a siloxane (Si–O–Si) network with surface silanol groups, SiH groups are known to form on silica surfaces under low-temperature or reducing conditions.[52–54] However, in the surface model employed in this study, a sufficient number of silanol groups are present, and the interfacial interactions are therefore dominated by these polar sites. Consequently, the presence of SiH groups is expected to have only a limited influence on the hydrophilicity and interfacial structure. Three different substrates were prepared by changing the cut-out positions and then used for the simulations. Averaged over the three amorphous silica substrates, the SiOH/SiH ratio of the silica surface was 0.85. The isosurface was constructed by scanning the surface with a probe of radius 0.15 nm, and the root-mean-square roughness was evaluated to be 0.11 nm. In a previous study, a crystalline silica surface with a surface roughness of 0.03 nm was also examined.[50] While a higher density was observed at the outermost interface on the substrate side for the crystalline surface, no difference was found in the curing reaction. A total of nine different initial structures were created for the MD simulations by placing three different epoxy/amine mixtures on each of three different silica substrates. Since the atomic coordinates of the substrate were constrained except for the surface functional groups, the NPT ensemble could not be applied. Moreover, using the NVT ensemble without a vacuum region would artificially suppress the curing shrinkage of thermoset systems. To reproduce the volume reduction during curing, a vacuum region was therefore introduced. Importantly, the epoxy resin did not expand into the vacuum region due to its cohesive interactions, and the density after curing agreed well with experimental values.[55,56]

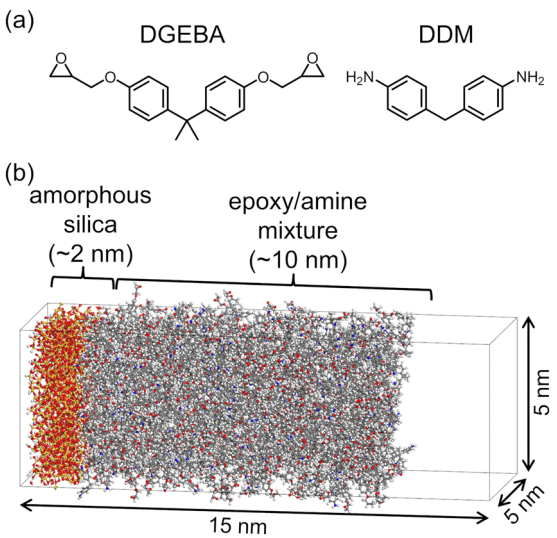

Fig. 1 (a) Chemical structures of epoxy and amine compounds. (b) Simulation system of epoxy/amine mixture on amorphous silica. The cell size is 5.0 × 5.0 × 15.0 nm^3. Carbon, oxygen, nitrogen, hydrogen, and silicon atoms are colored gray, red, blue, white, and ocher, respectively.

To investigate the aggregation states in the unreacted state, MD simulations were performed starting from the initial structure shown in Fig. 1(b). The simulations were run for 1 ns at 363 K with a time step of 1 fs under the NVT ensemble.[57] The Forcite module of Materials Studio 2025 (Dassault Systèmes) was used along with the COMPASS III force field.[58,59] For the silica substrate, the coordinates were constrained except for the hydrogen atoms of the surface SiH groups and the OH groups of SiOH.[50] Temperature control was achieved using a Nosé–Hoover-Langevin (NHL) thermostat, and electrostatic interactions were computed using the Particle–Particle Particle–Mesh (PPPM) algorithm. The van der Waals interactions were calculated using an atom-based summation method with a cutoff distance of 1.25 nm.

Epoxy and amine compounds react in two steps to form a three-dimensional network structure.[34] In the first step, an epoxy compound reacts with a primary amine to form a secondary amine, which subsequently reacts with another epoxy compound in the second step to form a tertiary amine.

The curing reaction between epoxy and amine compounds was investigated by MD simulation.[26,57,60] When the terminal carbon of an epoxy group and the nitrogen atom of an amino group approach within a reaction distance of 0.6 nm, an Arrhenius-type reaction probability k is defined as follows;

$$k = A \times \exp(-E_a/RT) \quad (1)$$

where A is an apparent frequency factor, set to 1×10^{18} to ensure that the curing reaction proceeds within a reasonable simulation time, E_a is the activation energy of the reaction, R is the gas constant, and T is the local temperature.[61] A random number was then generated and compared with this probability to determine whether a reaction will occur. To account for the temperature increase caused by the exothermic reaction, the heat of reaction (ΔH) was imparted as kinetic energy to the reacting molecules. This evaluation was performed every 0.01 ns, and the MD simulations were performed for 5 ns under the NVT ensemble at 363 K. The E_a and ΔH values for these reactions, determined by density functional theory (DFT) calculations, were 157.4 and 107.9 kJ mol^{-1} for the 1st-step reaction, and 147.7 and 108.7 kJ mol^{-1} for the 2nd-step reaction.

3. Results and discussion

In the curing reaction, the reaction conversion, defined as the consumption ratio of epoxy groups, progressed to an average of 80–87% for the entire system. Fig. 2(a) is a snapshot of the cured epoxy product at 80% reaction conversion. Each structure connected by chemical bonds was color-coded, with the largest network shown in blue. A continuous blue structure spanning the entire system can be clearly seen. A closer look revealed several small fragments of different colors, indicating the presence of unreacted isolated structures. Fig. 2(b) shows the dependence of the density of the unreacted epoxy/amine mixture and the reacted epoxy product (80% conversion) on the distance from the substrate at 363 K. Focusing first on the 4–7 nm bulk region, which is regarded as the bulk because the diffusion coefficient matches the bulk value and the orientation distribution is fully isotropic (see below), unaffected by either substrate or surface, the density increased from 1.09 g cm^{-3} to 1.12 g cm^{-3}, confirming shrinkage due to curing. In both unreacted and reacted cases, a peak was observed near the interface at a distance of 0.8 nm, and the density increased to about 1.25 g cm^{-3}. Here, the region within 1 nm from the substrate, in which the first density peak decays, is defined as the outermost interface on the substrate side. Similarly, an increase in density was observed at the outermost interface on the substrate side in the respective density profiles of the epoxy and amine compounds as shown in Fig. S1(a) (see SI). This is the result of packing due to molecular orientation, which will be discussed in detail later. Furthermore, amine compounds with a smaller molecular size segregated at the outermost interface on the substrate side as shown in Fig. S1(b) (see SI). On the surface at distances further than 8 nm from the substrate, the mixture was in a liquid state before the reaction and the surface was smooth. On the other hand, after curing, the surface became rougher due to the formation of cross-linked structures and the gradient of the density profile became more gradual.

The dependence of the progress of the curing reaction on the distance from the substrate was investigated. Fig. 3(a) shows the distribution of reacted epoxy groups at overall reaction conversion of 10% and 80% as a function of distance from the substrate. The distance from the substrate was divided into 0.5 nm intervals, and the reaction conversion evaluated

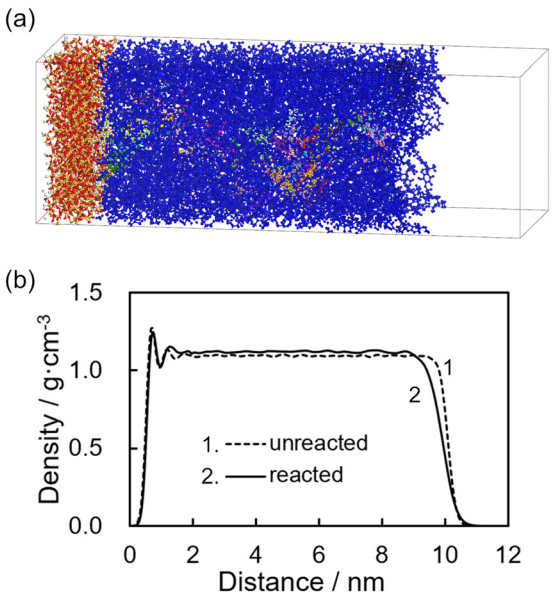

Fig. 2 (a) Snapshot of cured epoxy product at a reaction conversion of 80%. The epoxy structure is color-coded based on the covalent bond connectivity. (b) Dependence of density of epoxy/amine mixture on distance from substrate before and after curing reactions. The distance 0 corresponded to the position where the density of the mixture was zero.

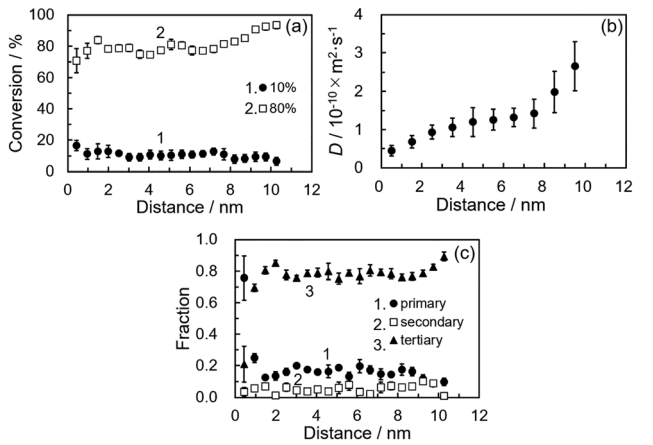

Fig. 3 (a) Distribution of reacted epoxy groups as a function of distance from the substrate at overall reaction conversions of 10% and 80%. (b) Diffusion coefficient of unreacted species as a function of distance from the substrate. (c) Dependence of primary, secondary, and tertiary amine fractions on distance from the substrate at 80% reaction conversion.

within each interval was defined as the local conversion. At an early-stage conversion of 10%, the local conversion increased to approximately 17% within 1 nm of the outermost interface on the substrate side. This is attributed to the segregation of amines at the interface, which provides more reaction partners for epoxy. Previous SFG spectroscopy studies have also reported faster reactions at the outermost interface on the substrate side, ascribed to the densification and orientation of reactive functional groups, supporting these results.[32] In contrast, at 80% conversion, the local conversion near the interface was about 10% lower than the system average, while conversion increased beyond 7 nm from the substrate. These trends reflect the distance-dependent mobility of unreacted species.

Fig. 3(b) shows the diffusion coefficient of unreacted species as a function of distance from the substrate. The system was divided into 1 nm layers, and the mean squared displacements (MSD) of epoxy and amine molecules initially in each layer were evaluated over a 1 ns MD simulation to calculate diffusion coefficients. In long MD simulations, molecules may migrate into adjacent regions. To minimize this effect, the MSD was calculated using short 1 ns trajectories. In the bulk region, the diffusion coefficient for 4–7 nm was close to $(1.08 \pm 0.07) \times 10^{-10}$ m^2 s^{-1}, obtained using a cubic cell under periodic boundary conditions. However, it decreased progressively closer to the substrate and was reduced to about 1/3 of the bulk value below 2 nm, reflecting suppressed mobility near the interface. In addition to the reduced diffusion coefficient, several other factors contribute to the slower interfacial reaction, including a reduced number of available reaction partners due to the presence of the substrate, local stoichiometric imbalance caused by preferential amine segregation, and steric constraints that limit the accessibility of epoxy groups. The interface therefore represents a diffusion-limited and accessibility-limited regime, leading to incomplete conversion. On the other hand, beyond 8 nm, the diffusion coefficient increased, consistent with the higher reaction conversion observed in the surface region.

To discuss the reaction state of the amine compounds, Fig. 3(c) shows the dependence of the fraction of primary, secondary, and tertiary amines on distance from the substrate at 80% reaction conversion. The fraction of primary amines increased markedly at the outermost interface on the substrate side below 1 nm and remained at 0.1–0.2 beyond this region. Secondary amines were present at fractions below 0.1 throughout all regions, and most had converted to tertiary amines by the end of the 1st step reaction, indicating progression to the 2nd step reaction. In contrast, tertiary amines exhibited low fractions at the outermost interface on the substrate side below 1 nm but increased to around 0.7–0.8 beyond this region, reaching up to 0.9 at distances greater than 9 nm. This behavior of tertiary amines was in good agreement with the reaction conversion profile at 80% shown in Fig. 3(a).

The orientation of molecules at the outermost interface on the substrate side within 1 nm from the substrate was then analyzed. As both DGEBA and DDM are anisotropic shaped molecules, they were expected to orient along the substrate.

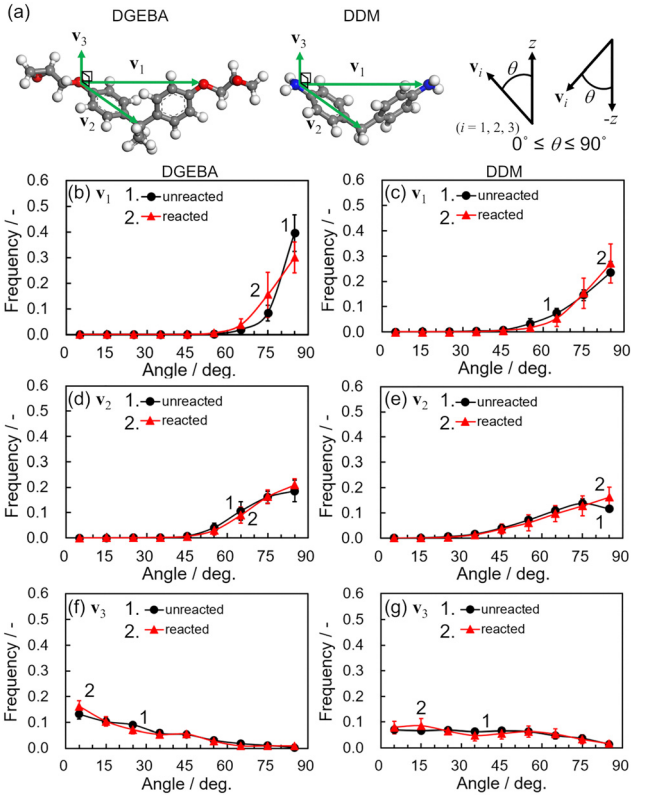

Fig. 4 (a) Definition of vector $\mathbf{v}_1$ along the principal axis of the molecule, vector $\mathbf{v}_2$ along the phenyl group, and vector $\mathbf{v}_3$ as the normal to the plane formed by $\mathbf{v}_1$ and $\mathbf{v}_2$. The orientation angle θ was measured from the z-axis perpendicular to the substrate. Frequency distributions of orientation angles: (b) and (c) $\mathbf{v}_1$, (d) and (e) $\mathbf{v}_2$, and (f) and (g) $\mathbf{v}_3$ for DGEBA and DDM.

Thus, as shown in Fig. 4(a), three orthogonal vectors were defined to characterize molecular orientation. Vector $\mathbf{v}_1$ was defined along the principal molecular axis, corresponding to the direction connecting the ether oxygen atoms for DGEBA and nitrogen atoms for DDM. Vector $\mathbf{v}_2$ was defined along the phenyl group, as the vector connecting the central carbon atom to the ether oxygen or nitrogen atom. Vector $\mathbf{v}_3$ was defined as the normal to the plane spanned by $\mathbf{v}_1$ and $\mathbf{v}_2$. Although phenyl rings undergo thermal rotation around $\mathbf{v}_2$, this rotational motion does not alter the direction of $\mathbf{v}_2$ itself. The angle θ between the z-axis and the vector extending from the substrate toward the epoxy resin side, or equivalently from the $-z$-axis, was evaluated. Since the orientation was symmetrical around 90° when evaluated over 0–180° from the z-axis, the orientation along the substrate was considered in the range of 0–90°. Fig. 4(b) shows the orientational frequency of vector $\mathbf{v}_1$ along the principal axis of the DGEBA before and after the curing reaction. The orientation angles were plotted in 10° increments, counting the number of occurrences within each range and plotting their frequency. Before the reaction, the frequency increased as it approached 90°, indicating strong in-plane orientation of the substrate. After the reaction, although the in-plane orientation was maintained, the orientation distribution became slightly broader. Our previous study revealed that DGEBA monomers oriented toward the substrate became

constrained upon incorporation into the cross-linked structure during the reaction and could no longer orient as freely as before, which is in good agreement with the present result.[26] Fig. 4(c) shows that DDM, similar to DGEBA, also orients its principal axis parallel to the substrate. However, compared to DGEBA, the molecular principal axis of DDM is shorter and less anisotropic, resulting in a lower degree of orientation before the reaction, which remained almost unchanged even after the reaction. This behavior is attributed to the greater molecular flexibility of DDM, arising from its smaller molecular size and the absence of the two methyl groups at the molecular center present in DGEBA.

Fig. 4(d and e) show the orientational frequency of vector $\mathbf{v}_2$, defined along the phenyl group for DGEBA and DDM, respectively. Although less marked than that of the principal axis, in-plane orientation was observed near 90° both before and after the reaction, and it was stronger in DGEBA than in DDM, similar to $\mathbf{v}_1$. In both epoxy and amine compounds, when one phenyl ring aligns parallel to the substrate, the other ring becomes tilted due to the molecular geometry of DGEBA and DDM, resulting in a broader angular distribution. The in-plane orientation of $\mathbf{v}_1$ and $\mathbf{v}_2$ contributed to the increase in density at the outermost interface on the substrate side, as shown in Fig. 2(b).

Fig. 4(f) shows the orientation frequency of vector $\mathbf{v}_3$ for DGEBA, which exhibits a slight increase toward 0°, suggesting that the plane formed by $\mathbf{v}_1$ and $\mathbf{v}_2$ tends to align slightly with the substrate. This is reasonable given the presence of methyl groups bonded to the central carbon atom of the DGEBA molecule, together with the size and bond angles of these methyl groups. In contrast, as shown in Fig. 4(g), the orientation frequency of vector $\mathbf{v}_3$ for DDM was broadly distributed. This result indicates that while DDM molecules orient their principal axis and phenyl group along the substrate, they are less constrained around the principal axis. This behavior is likely attributable to the smaller molecular size of DDM and the absence of methyl groups attached to its central carbon atom.

The relationship between the initial orientation of the molecules at the outermost interface on the substrate side and the time at which the reaction occurred was then investigated. Fig. 5 shows the relationship between the reaction time and the initial orientation angle for $\mathbf{v}_1$ (a and b), $\mathbf{v}_2$ (c and d) and $\mathbf{v}_3$ (e and f). First, the dependence of reaction time on the initial orientation angle was evaluated. For both $\mathbf{v}_1$ and $\mathbf{v}_2$, groups oriented at angles above 60° reacted at similarly early stages, with no significant differences observed. However, in DDM, molecules whose principal axis (50–60°) and phenyl groups (30–40°) were weakly oriented along the substrate tended to react more slowly as shown in Table S1 (See SI). Thus, the slower reaction of these groups does not arise simply from their lower population, but rather reflects their reduced accessibility within the interfacial environment. In contrast, no such tendency was observed in DGEBA. This is likely because molecules oriented at the outermost interface on the substrate side can readily find reaction partners, whereas the number of available partners decreases with increasing distance from the

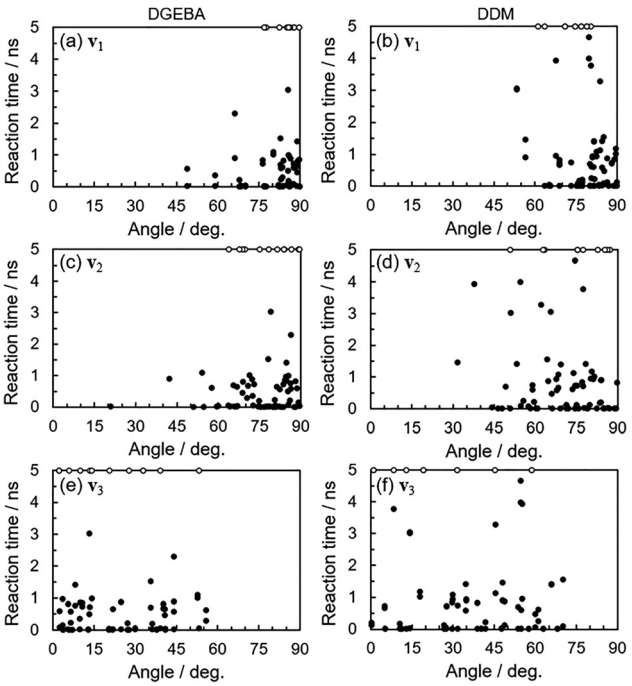

Fig. 5 Relationship between the reaction time and the initial orientation angle for molecules at the outermost interface on the substrate side; (a) and (b) $\mathbf{v}_1$, (c) and (d) $\mathbf{v}_2$, and (e) and (f) $\mathbf{v}_3$ for DGEBA and DDM, respectively. White symbols at 5 ns indicate molecules that did not react.

interface.[32] Next, these results indicate that a large number of molecules reacted very early (~0.03 ns). Counting molecules that reacted by 0.03 ns, the percentage was 29.7 ± 2.9% for DGEBA and 28.0 ± 6.3% for DDM. Similarly, the relationship between the initial orientation of the molecules and the reaction time was investigated for the bulk region, which is about 5 nm away from the substrate as shown in Fig. S2 (see SI). In the bulk region, the orientation of the molecules was isotropic, which is to be expected as there is no restraint from the substrate. Furthermore, the percentage of molecules that reacted by 0.03 ns was 16.9 ± 2.2% for DGEBA and 17.6 ± 2.3% for DDM, which was considerably lower than at the outermost interface on the substrate side.

The interaction between the silica surface and specific functional groups was investigated. Fig. 6(a) shows the radial

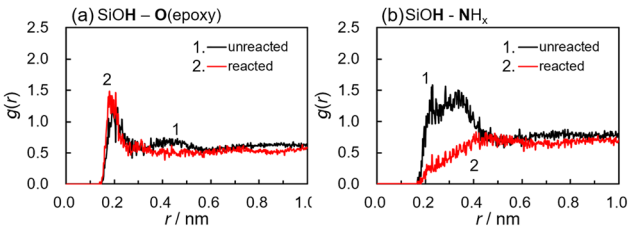

Fig. 6 (a) Radial distribution function between hydrogen atoms of SiOH groups on the silica surface and oxygen atoms of epoxy groups before and after the reaction. (b) Radial distribution function between hydrogen atoms of SiOH groups on the silica surface and nitrogen atoms of amines before and after the reaction.

distribution function between the hydrogen atoms of the SiOH groups and the oxygen atoms of the epoxy groups before the reaction or the COH groups after the reaction. Even before the reaction, a peak appeared at 0.2 nm, corresponding to the typical hydrogen bonding distance, and this peak became more pronounced after the reaction. This makes it clear that the reaction opens an epoxy ring to form a COH group, which subsequently forms a hydrogen bond with a SiOH group. While hydrogen bonding is expected to enhance the alignment of vector $\mathbf{v}_1$ along the substrate, as depicted in Fig. 4(b), it competes with the constraint caused by incorporation into the cross-linked structure, and the results suggest that the latter is dominant.

On the other hand, Fig. 6(b) shows the radial distribution function between the hydrogen atoms of the SiOH groups and the nitrogen atoms of the amine compounds. Before the reaction, a broad peak was observed at 0.2 to 3.5 nm, indicating that the amino groups strongly interacted with the SiOH groups through hydrogen bond formation. Because amines segregate at the outermost interface on the substrate side, SiOH–NH_2 correlations slightly longer than typical hydrogen-bonding distances were also included in the distribution. However, this peak disappeared after the reaction. This is because the amines were transformed into secondary and subsequently tertiary amines by the reaction, resulting in a reduced charge on the nitrogen atoms and thus weaker interactions with the SiOH groups, as well as their incorporation into the cross-linked structure, which prevented them from freely orienting. This change in hydrogen bonding has little effect on the orientation of DDM, as shown in Fig. 4(c).

Fig. 7(a) shows a snapshot near the interface at a reaction conversion of 87%. In the cured epoxy product, each structure connected by chemical bonds is color-coded, with the blue network spanning the entire system. However, small isolated fragments (low-molecular-weight components not bonded to the main network) and unreacted monomers remain near the interface.[57] Fig. 7(b) shows a bottom view of the same epoxy product cured to 87% from the substrate side. As indicated by the arrows in the figure, unreacted monomers of epoxy and amine compounds, as well as small isolated fragments, were present at the outermost interface on the substrate side. This is attributed to the lower reaction conversion achieved at the outermost interface on the substrate side, and the presence of excess amines deviating from the stoichiometric ratio. Considering that these species are surrounded by the cross-linked network and that diffusion is suppressed, it is unlikely that further reactions will occur. In fact, MD simulations of the curing reaction were extended up to 10 ns but no further reactions occurred at the interface. Although similar unreacted monomers and isolated fragments can also be observed in the bulk when the reaction conversion is low, they become scarcely visible once the reaction conversion exceeds 80%. However, due to geometric constraints, the reaction conversion cannot reach 100%, and unreacted monomers and small isolated fragments do not completely disappear even in the bulk. In this study, MD simulations were conducted using amorphous silica as the substrate. Even if the properties of the substrate surface are altered, although the strength of hydrogen bonding with the cured epoxy changes depending on its hydrophilicity, the presence of an incompletely cross-linked structure at the outermost interface on the substrate side remains unchanged.[26]

The molecular configuration shown in Fig. 7, obtained from MD snapshots, was representative of all simulation conducted under different initial conditions. Fig. 8 shows a schematic illustration of the cured epoxy product near the solid interface in the cross-sectional direction, drawn based on the results described above. At the outermost interface on the substrate side, within 1 nm from the substrate, the molecules are oriented in-plane along the substrate, resulting in improved packing and densification. In addition, amine compounds with smaller molecular size segregate, leading to a deviation from the stoichiometric ratio. Near the interface, the reaction proceeds rapidly in the initial stage, up to a reaction conversion of 10%, because the epoxy has more reaction partners. SFG spectroscopy results have also reported faster reactions at the outermost interface on the substrate side, which were explained in terms of the densification and orientation of reactive functional groups.[32] However, thereafter, the reaction slows down due to the suppression of molecular motion, resulting in the presence of unreacted epoxy and amine monomers, as well as small fragments that have only slightly reacted, existing in isolation.[24] Even if excess amines are incorporated into the main cross-linked structure, many of them react only with functional groups on one side of the molecule due to the limited availability of epoxies as reaction partners. This asymmetry ultimately leads to the formation of dangling chains,

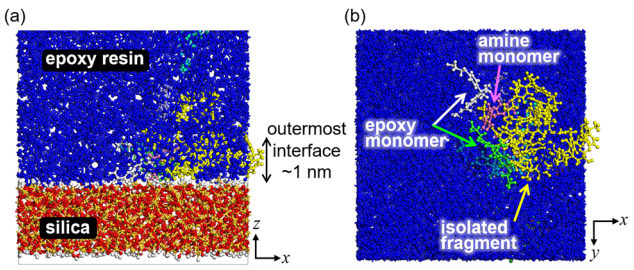

Fig. 7 (a) Snapshot near the interface at 87% reaction conversion. (b) Bottom view of the cured epoxy product.

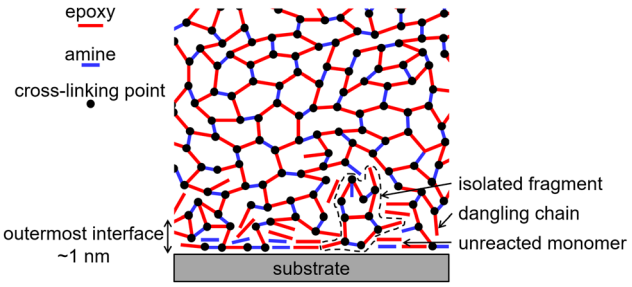

Fig. 8 Schematic illustration of the molecular picture of a cured epoxy product in the vicinity of the solid interface.

defined as epoxy or amine molecules connected to the main network through only one reacted end.[57]

Finally, based on the molecular picture of the cured epoxy product at the interface revealed in this study, the relationship with adhesive properties is discussed. When the cured epoxy product is separated from the adherend surface, the main cross-linked structure transfers the applied force. Unreacted monomers and isolated fragments present at the interface are considered to contribute little to adhesion because they are not connected to the main cross-linked structure. Although dangling chains are connected to the main cross-linked structure, they are less effective in resisting deformation. The presence of unreacted monomers, isolated chains, and dangling chains is detrimental to adhesion and is indicative of the formation of a weak boundary layer.[62,63] Therefore, material design and control of the curing process are required to reduce such incomplete cross-linked structures. We recently reported that maintaining stoichiometry can reduce isolated low-molecular weight components and dangling chains.[57] One approach is to align the molecular sizes of the epoxy and amine compounds to prevent the segregation of amine. The validity of this concept has been supported by our MD simulations and will be experimentally verified in future studies.[34]

4. Conclusions

We identified the local heterogeneous aggregation state of a cured epoxy product at the interface with amorphous silica. At the outermost interface on the substrate side, the density increased due to molecular orientation and packing, with a maximum at 0.8 nm, and the effect extended down to 2 nm. Both the epoxy and amine compounds have an anisotropic shape so the molecular principal axis and the phenyl groups in the molecule were oriented in a plane parallel to the substrate, although they were less constrained around the principal axis. The orientation angle of selectively fast reacting molecules was not observed, however, a higher percentage of molecules reacted in the very early stage at the outermost interface on the substrate side compared to the bulk. This density heterogeneity near the interface was similarly maintained after the reaction. The interaction between the silica surface and the epoxy groups was further strengthened by the reaction to a COH group. Amines also interacted with the silica surface, however, after the reaction they became tertiary amines, which made them weaker than before the reaction. At a distance over 2 nm from the substrate, the density was the same as in the bulk. Amine compounds with a smaller molecular size segregated in the region 1 nm from the substrate. This resulted in an excess of reacting partners for the epoxy compound at the outermost interface on the substrate side, leading to faster progress of the initial stage of the curing reaction. However, due to the suppression of the molecular motion of unreacted substances in the vicinity of the interface, the subsequent reaction progress was slower in the region less than 2 nm from the substrate and the final reaction conversion was about 10% lower than in the bulk. At the outermost interface on the substrate side, the molecular picture was obtained, with unreacted monomers and small isolated fragments remaining.

Conflicts of interest

There are no conflicts to declare.

Data availability

The data supporting this article will be available upon request at https://www.cstf.kyushu-u.ac.jp/~tanaka-lab/english/.

Supplementary information (SI): density profile and relationship between reaction time and molecular orientation. See DOI: https://doi.org/10.1039/d5sm01089f.

Acknowledgements

This research was supported by JST-Mirai Program Grant Number JPMJMI18A2, Japan.

Notes and references

1 F.-L. Jin, X. Li and S.-J. Park, *J. Ind. Eng. Chem.*, 2015, **29**, 1–11.
2 T. Vidil, F. Tournilhac, S. Musso, A. Robisson and L. Leibler, *Prog. Polym. Sci.*, 2016, **62**, 126–179.
3 M. Bakir, J. L. Meyer, S. Pang, J. Economy and I. Jasiuk, *Soft Matter*, 2020, **16**, 1389–1403.
4 H. Zheng, W. Zhang, B. Li, J. Zhu, C. Wang, G. Song, G. Wu, X. Yang, Y. Huang and L. Ma, *Composites, Part B*, 2022, **233**, 109639.
5 B. Du, X. Zhou, Q. Li, J. Liu, Y. Liu, X. Zeng, X. Cheng and H. Hu, *ACS Omega*, 2023, **8**, 39984–40004.
6 T. Hoshino, Y. Okamoto, A. Yamamoto and H. Masunaga, *Soft Matter*, 2023, **19**, 3267–3272.
7 P. K. Jani, B. V. Farias, R. K. Jain, K. R. Houston, O. D. Velev, E. E. Santiso, L. C. Hsiao and S. A. Khan, *Macromolecules*, 2024, **57**, 2130–2141.
8 C. Declet-Perez, E. M. Redline, L. F. Francis and F. S. Bates, *ACS Macro Lett.*, 2012, **1**, 338–342.
9 H. Li, Y. Q. Li, Y. You and H. B. Xie, *ACS Macro Lett.*, 2024, **13**, 775–780.
10 J. Li, Z. Zou, Y. Lai, Y. Wu, M. Chen, X. Zhao and Z. Chen, *ACS Macro Lett.*, 2024, **13**, 1483–1489.
11 B. R. Hafner, S. Pal, B. Lewis, S. Keten and K. R. Shull, *ACS Macro Lett.*, 2024, **13**, 1545–1550.
12 S. Sprenger, *J. Mater. Sci.*, 2014, **49**, 2391–2402.
13 J. J. Chruściel and E. Leśniak, *Prog. Polym. Sci.*, 2015, **41**, 67–121.
14 N. Khatavkar and B. Kandasubramanian, *RSC Adv.*, 2016, **6**, 6709–6718.
15 P. Uniyal, P. Gaur, J. Yadav, N. A. Bhalla, T. Khan, H. Junaedi and T. A. Sabaey, *ACS Omega*, 2025, **10**, 15810–15839.

16 Ö. Dağlar, T. Türel, C. Pantazidis and Ž. Tomović, *Macromol. Rapid Commun.*, 2025, **46**, 2400678.
17 R. Dinu, U. Lafont, O. Damiano, F. Orange and A. Mija, *ACS Appl. Polym. Mater.*, 2023, **5**, 2542–2552.
18 K. Aragishi, Y. Takeda, Y. Suzuki and A. Matsumoto, *Polym. J.*, 2024, **56**, 529–540.
19 M. J. Stevens, *Macromolecules*, 2001, **34**, 2710–2718.
20 K. W. Putz, M. J. Palmeri, R. B. Cohn, R. Andrews and L. C. Brinson, *Macromolecules*, 2008, **41**, 6752–6756.
21 J. Baller, N. Becker, M. Ziehmer, M. Thomassey, B. Zielinski and U. Müller, *Polymer*, 2009, **50**, 3211–3219.
22 B. I. Dach, H. R. Rengifo, N. J. Turro and J. T. Koberstein, *Macromolecules*, 2010, **43**, 6549–6552.
23 S. Mandal, R. Raj, K. Samanta, S. Kumar and S. Bose, *ACS Appl. Mater. Interfaces*, 2024, **16**, 31877–31894.
24 T. Hirai, K. Kawasaki and K. Tanaka, *Phys. Chem. Chem. Phys.*, 2012, **14**, 13532–13534.
25 Z. Cao, Q. Bian, Y. Chen, F. Liang and G. Wang, *ACS Macro Lett.*, 2017, **6**, 1124–1128.
26 S. Yamamoto, R. Kuwahara and K. Tanaka, *ACS Appl. Polym. Mater.*, 2022, **4**, 6038–6046.
27 F. Zhang, D. Liu, R. Yang and D. Lu, *Macromolecules*, 2024, **57**, 4648–4661.
28 J. L. Lenhart and W.-L. Wu, *Macromolecules*, 2002, **35**, 5145–5152.
29 S. Mani and R. Khare, *Macromolecules*, 2018, **51**, 576–588.
30 S. Saeki, H. Taneda, T. Abe and K. Tanaka, *Langmuir*, 2025, **41**, 10668–10675.
31 A. V. Vázquez, B. Holden, C. Kristalyn, M. Fuller, B. Wilkerson and Z. Chen, *ACS Appl. Mater. Interfaces*, 2011, **3**, 1640–1651.
32 K. Yamaguchi, D. Kawaguchi, N. Miyata, T. Miyazaki, H. Aoki, S. Yamamoto and K. Tanaka, *Phys. Chem. Chem. Phys.*, 2022, **24**, 21578–21582.
33 Y. Liu, N. Miyata, T. Miyazaki, A. Shundo, D. Kawaguchi, K. Tanaka and H. Aoki, *Langmuir*, 2023, **39**, 10154–10162.
34 S. Yamamoto and K. Tanaka, *Macromol. Rapid Commun.*, 2025, **46**, 2400978.
35 A. V. Vázquez, A. P. Boughton, N. E. Shephard, S. M. Rhodes and Z. Chen, *ACS Appl. Mater. Interfaces*, 2010, **2**, 96–103.
36 T. Ge, G. S. Grest and M. O. Robbins, *ACS Macro Lett.*, 2013, **2**, 882–886.
37 T. Okabe, T. Takehara, K. Inose, N. Hirano, M. Nishikawa and T. Uehara, *Polymer*, 2013, **54**, 4660–4668.
38 K. S. Khare and C. F. Abrams, *Soft Matter*, 2021, **17**, 9957–9966.
39 G. M. Odegard, S. U. Patil, P. S. Gaikwad, P. Deshpande, A. S. Kreig, S. P. Shah, A. Reyes, T. Dickens, J. A. King and M. Maiaru, *Soft Matter*, 2022, **18**, 7550–7558.
40 S. Morsch, C. R. Wand, S. Gibbon, M. Irwin, F. Siperstein and S. Lyon, *Appl. Surf. Sci.*, 2023, **609**, 155380.
41 S. H. Kwon, H. Kang, B.-J. Kim, H. I. Lee, J. M. Lee, J. Kim and S. G. Lee, *Sci. Rep.*, 2023, **13**, 138.
42 K. Harris, C. R. Wand, P. Visser and F. R. Siperstein, *RSC Appl. Interfaces*, 2024, **1**, 812–820.
43 Y. Kawagoe, G. Kikugawa, S. Komori, K. Shirasu and T. Okabe, *Thermochim. Acta*, 2025, **747**, 179949.
44 D. J. Eyckens, J. L. Adcock, J. P. Blinco, K. E. Fairfull-Smith, J. Harris, F. Vuković, S. He, B. Dharmasiri, T. R. Walsh, P. S. Francis, A. Hendlmeier and L. C. Henderson, *Macromol. Rapid Commun.*, 2025, **46**, 2300274.
45 R. Zheng, T. C. Germann, M. Gross and M. Mehana, *ACS Sustainable Chem. Eng.*, 2024, **12**, 5555–5563.
46 C.-H. Chung, L.-T. Wu, D. M. Sentosa, C.-C. Ho, P.-W. Chi, W.-C. Hsu, K.-W. Yeh, C.-C. Chang, B. J. Hwang, M.-K. Wu, J.-C. Jiang, C.-C. Hu and Y.-C. Chiu, *ACS Appl. Mater. Interfaces*, 2025, **17**, 23872–23884.
47 Y. Shen, C. Li, D. Yu, X. Zhu and X. Zou, *ACS Appl. Mater. Interfaces*, 2025, **17**, 27530–27544.
48 X. Cheng, T. Yan, D. Qin, L. Leng, J. Tian, T. Sun, J. Lu, X. Liu and Y. Zhang, *ACS Appl. Mater. Interfaces*, 2025, **17**, 13988–13996.
49 M. Krinninger, F. Kraushofer, N. B. Refvik, M. Blum and B. A. J. Lechner, *ACS Appl. Mater. Interfaces*, 2024, **16**, 27481–27489.
50 S. Yamamoto, R. Kuwahara and K. Tanaka, *Nihon Reoroji Gakkaishi*, 2024, **52**, 91–98.
51 S. Yamamoto, Y. Tsuji, R. Kuwahara, K. Yoshizawa and K. Tanaka, *Langmuir*, 2024, **40**, 12613–12621.
52 M. Chorro, C. Chorro, O. Dolladille, S. Partyka and R. Zanna, *J. Colloid Interface Sci.*, 1999, **210**, 134–143.
53 F. Ojeda, I. Montero, F. Abel and J. M. Albella, *Chem. Mater.*, 2001, **13**, 3986–3992.
54 N. Plumeré, B. Speiser, B. Dietrich, K. Albert, J. J. Pesek and M. T. Matyska, *Langmuir*, 2009, **25**, 13481–13487.
55 A. N. Rissanou and V. Harmandaris, *Macromolecules*, 2015, **48**, 2761–2772.
56 Z. Khaknejad, N. Mehdipour and H. Eslami, *ChemPhysChem*, 2020, **21**, 1134–1145.
57 S. Yamamoto, N. T. Phan, K. Kihara, A. Shundo and K. Tanaka, *Polym. J.*, 2025, **57**, 357–366.
58 M. Meunier and S. Robertson, *Mol. Simul.*, 2021, **47**, 537–539.
59 R. L. C. Akkermans, N. A. Spenley and S. H. Robertson, *Mol. Simul.*, 2021, **47**, 540–551.
60 T. Miyata, Y. K. Sato, Y. Kawagoe, K. Shirasu, H.-F. Wang, A. Kumagai, S. Kinoshita, M. Mizukami, K. Yoshida, H.-H. Huang, T. Okabe, K. Hagita, T. Mizoguchi and H. Jinnai, *Nat. Commun.*, 2024, **15**, 1898.
61 S. Yamamoto and K. Tanaka, *Nihon Reoroji Gakkaishi*, 2021, **49**, 55–56.
62 J. J. Bikerman, *The Science of Adhesive Joints*, Academic, New York, 1968.
63 A. A. Shcherbina, Y. Y. Gladkikh and A. E. Chalykh, *Polym. Sci., Ser. A*, 2012, **54**, 375–384.

